LoCoRand: Modeling Location and Contention Randomness for Node-Assisted WiFi Backscatter Communication (Supplementary Material)

Yulei Wang, Qinglin Zhao, *Senior Member, IEEE*, Shumin Yao, MengChu Zhou, *Fellow, IEEE*, Li Feng, and Peiyun Zhang, *Senior Member, IEEE*

Appendix A: Details of TABLE I

For ease of reference, we summarize all the used notations in Table I along with their corresponding descriptions.

TABLE I
NOTIONS AND THEIR DESCRIPTIONS

Notation	Description
	WiFi nodes
Φ_w^0/λ_w^0	The HPPP Φ_w^0 of underlying nodes with density λ_w^0
$\Phi_w/\Phi_w^a/\lambda_w$	MHCPP Φ_w/approximated PPP Φ_w^a of nodes with density λ_w
Φ_w'/λ_w'	The set of non-transmitting nodes except w with density λ_w'
$\tilde{d}/\lvert\tilde{A}\rvert$	The radius/area of subcell $\tilde{A}$
$\check{d}$	The minimum distance between any two nodes
$M/\hat{m}$	The number of nodes in one cell with maximum value $\hat{m}$
$\mathbb{P}(m)$	The probability that there are m nodes in one cell
$\mathbb{P}_w^m$	The successful probability of one node-to-AP transmission
Ω	The generic slot duration representing the elapsed time of one backoff decrement in WiFi contention
ω	The duration of a basic slot for nodes
T_m^s	The time duration for a successful WiFi transmission
T_m^c	The time duration for an unsuccessful WiFi transmission
τ	The attempt rate of each node
γ	The collision probability experienced by each node
$\check{C}$	The minimum contention window size
K	The maximum backoff stage for nodes
$\mathbb{P}_w(Idle)$	The probability that the channel is idle for nodes
$\mathbb{P}_w(Succ)$	The probability of a successful WiFi transmission
$\mathbb{P}_w(Coll)$	The probability of a WiFi collision
$P_{b,w}$	The received desired signal power at node w from tag b
I	The received interfering signal power from tags
θ	The predefined SINR threshold
$R_{b,w}$	The distance between tag b and node w
$R_{b',w}$	The distance between interfering tag b' and node w
$f(\mathbf{y}\|\mathbf{x})$	The conditional probability density function of $\mathbf{y}$ given an $\mathbf{x}$
$\tilde{f}_{R_{b,w}}(r_{b,w})$	The probability density function of $R_{b,w}$
$\Gamma_w^m(\cdot)$	The WiFi throughput when there are m nodes in one cell
ξ	The number of successfully transmitted bits by nodes in one cell, during a unit time
Γ_w	The average WiFi throughput
	Backscatter tags
Φ_b/Λ_b	The MCP Φ_b of tags with mean Λ_b tags in one subcell
$\Phi_b'/\bar{\Psi}$	The set of interfering tags with mean $\bar{\Psi}$ tags in one subcell
P_0	The reflection power of each tag
H	The channel power gain of small-scale fading
α	The path-loss exponent
σ^2	Additive white Gaussian noise with variance σ^2
$N/\hat{n}$	The number of tags in a subcell with maximum value $\hat{n}$
$\mathbb{P}(n)$	The probability that there are n tags in a subcell
$\Psi/\bar{\Psi}$	Number/Mean # of tags that transmit concurrently in a subcell
η	The number of successfully transmitted bits by tags within all subcells, during a unit time
	(Continued)

Table I (continued)	
Γ_b	The average backscatter throughput
L	The number of busy tones for tags
$\mathbb{P}_b^s$	The probability of a successful backscatter transmission
AP	
$d/\|A\|$	The radius/area of cell A
System	
Γ_s	The average system throughput

Appendix B: Realization of spatial distributions of AP, nodes and tags

Fig. 1 depicts a realization of spatial distributions of AP, underlying nodes following an HPPP Φ_w^0, retained nodes following an MHCPP Φ_w, and tags following an MCP Φ_b.

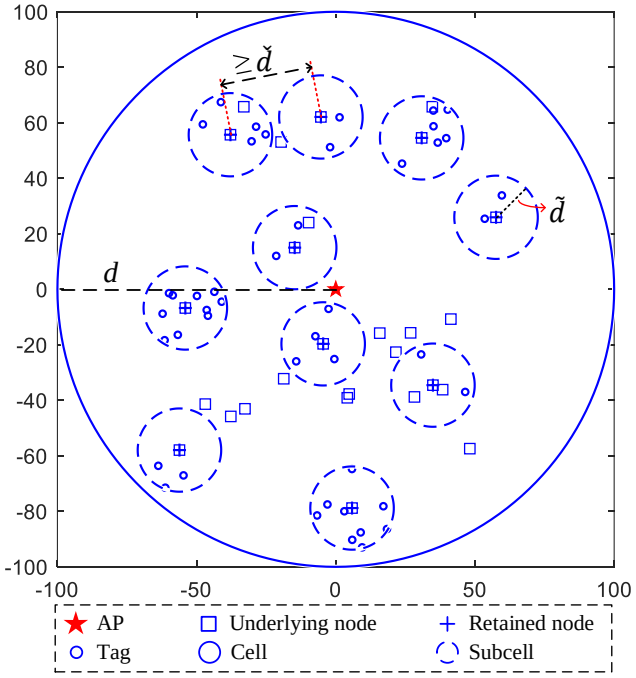

Fig. 1. A realization of spatial distributions of AP, underlying nodes following an HPPP Φ_w^0, retained nodes following an MHCPP Φ_w, and tags following an MCP Φ_b, where d = 100 m, $\tilde{d}$ = 15 m, $\check{d}$ = 30 m, λ_w^0 = 0.001 nodes/m^2, and Λ_b = 5 tags.

Appendix C: Calculation of τ, $\mathbb{P}_w(Succ|m)$, $\mathbb{E}[\Omega|m]$

Here, we proceed to give the expressions of $\mathbb{P}_w(Succ|m)$ and $\mathbb{E}[\Omega|m]$, since they are also used in the calculation of backscatter throughput in Section VI in the paper. Let τ denote the rate that each node attempts to transmit a packet when m nodes contend for the channel. In the following, we calculate τ, $\mathbb{P}_w(Succ|m)$, and $\mathbb{E}[\Omega|m]$ sequentially.

A. Calculation of τ

For a single-cell WiFi network with m nodes, the attempt rate τ is governed by the following fixed-point equation [1], [2]:

$$\begin{cases} \tau = \dfrac{2}{1+\check{C}+\gamma\check{C}\sum_{k=0}^{K-1}(2\gamma)^k} \\ \gamma = 1-(1-\tau)^{m-1} \end{cases} \tag{1}$$

where γ denotes the collision probability that each node experiences in channel contention, $\check{C}$ and K are the minimum contention window and the maximum backoff stage, respectively.

B. Calculation of $\mathbb{P}_w(Succ|m)$

In WiFi, one node-to-AP transmission is successful when only one among m nodes attempts to transmit a packet. Hence, $\mathbb{P}_w(Succ|m)$ can be expressed as

$$\mathbb{P}_w(Succ|m) = m\tau(1-\tau)^{m-1}. \tag{2}$$

C. Calculation of $\mathbb{E}[\Omega|m]$

In WiFi, time is divided into a series of basic slots, where a basic slot is the predefined minimum time unit. Given m, the generic slot duration, $\Omega|m$, depends on whether one basic slot is idle, and whether one transmission is successful or unsuccessful. We have

$$\Omega|m = \begin{cases} \omega & \mathbb{P}_w(Idle|m) \\ T_m^s & \mathbb{P}_w(Succ|m) \\ T_m^c & \mathbb{P}_w(Coll|m) \end{cases} \tag{3}$$

where ω is the duration of a basic slot, $\mathbb{P}_w(Succ|m)$ is given in (2), and other variables are defined as follows.

- T_m^s is one successful WiFi transmission time, including packet transmission time T_{Packet}, SIFS time T_{SIFS}, ACK time T_{ACK}, and DIFS time T_{DIFS}. Hence, we have:
$$T_m^s = T_{Packet} + T_{SIFS} + T_{ACK} + T_{DIFS}. \tag{4}$$
- T_m^c is one unsuccessful WiFi transmission time, i.e.,
$$T_m^c = T_{Packet} + T_{ACKTimeout} + T_{DIFS} \tag{5}$$
where $T_{ACKTimeout}$ is one AckTimeout time and can be set to $T_{ACK} + T_{SIFS}$ [3].
- $\mathbb{P}_w(Idle|m)$ is the probability that a basic slot is idle, namely, the probability that none among m nodes attempt to transmit a packet in one basic slot. We have
$$\mathbb{P}_w(Idle|m) = (1-\tau)^m. \tag{6}$$
- $\mathbb{P}_w(Coll|m)$ is the probability that one node experiences a collision when m nodes contend for the channel and is given as:
$$\mathbb{P}_w(Coll|m) = 1 - \mathbb{P}_w(Idle|m) - \mathbb{P}_w(Succ|m) \tag{7}$$

From (3)**Error! Reference source not found.**, we can easily express $\mathbb{E}[\Omega|m]$:

$$\mathbb{E}[\Omega|m] = \omega\mathbb{P}_w(Idle|m) + T_m^s\mathbb{P}_w(Succ|m) + T_m^c\mathbb{P}_w(Coll|m). \tag{8}$$

Appendix D: Calculation of $\mathbb{P}(\boldsymbol{\Psi = \psi|n})$

Fig. 2 presents an intuitive illustration of the calculation of $\mathbb{P}(\Psi = \psi|n)$.

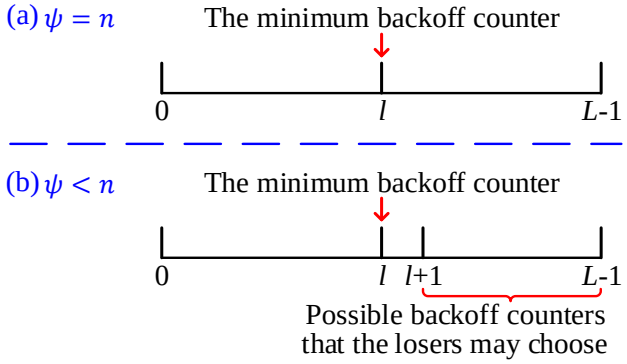

Fig. 2. Calculation of $\mathbb{P}(\Psi = \psi|n)$.

Appendix E: Derivations of $\mathcal{L}_I(s)$ and its asymptotic lower bound $\mathcal{L}_I'(s)$

Here, we first express $\mathbb{E}_I\left[\mathbb{P}\left(SINR\left(r_{b,w}, I\right) > \theta\right)\right]$ as

$$\begin{aligned}
&\mathbb{E}_I\left[\mathbb{P}\left(SINR\left(r_{b,w}, I\right) > \theta\right)\right] = \mathbb{E}_I\left[\mathbb{P}\left(\frac{P_0 H_{b,w} r_{b,w}^{-\alpha}}{I+\sigma^2} > \theta\right)\right] \\
&= \mathbb{E}_I\left[\mathbb{P}\left(H_{b,w} > \frac{\theta r_{b,w}^{\alpha}(I+\sigma^2)}{P_0}\right)\right] \\
&= 1 - \mathbb{E}_I\left[F_{H_{b,w}}\left(\frac{\theta r_{b,w}^{\alpha}}{P_0}(I+\sigma^2)\right)\right] \\
&\overset{(a)}{=} \mathbb{E}_I\left[\exp\left(-\frac{\mu\theta r_{b,w}^{\alpha}}{P_0}(I+\sigma^2)\right)\right] \\
&= \exp\left(-\frac{\mu\theta r_{b,w}^{\alpha}}{P_0}\sigma^2\right)\mathbb{E}_I\left[\exp\left(-\frac{\mu\theta r_{b,w}^{\alpha}}{P_0}I\right)\right] \\
&\overset{(b)}{=} \exp(-s\sigma^2)\cdot\mathcal{L}_I(s)
\end{aligned} \tag{9}$$

where (a) holds because $H_{b,w}$ follows an exponential distribution with mean $1/\mu$, i.e., $H_{b,w}\sim \mathrm{Exp}(\mu)$. Eq. (b) holds because the Laplace transform of the interference I, $\mathcal{L}_I(s)=\mathbb{E}[\exp(-sI)]$, where $s=\frac{\mu\theta r_{b,w}^{\alpha}}{P_0}$. Note that the interference I that node w suffers depends on the set of interfering tags Φ_b'. We next calculate $\mathcal{L}_I(s)$.

1) Calculation and asymptotic lower bound of $\mathcal{L}_I(s)$

Taking into account Φ_b', we can obtain:

$$\begin{aligned}\mathcal{L}_I(s)&=\mathbb{E}_{R_{b',w},H_{b',w}}\left[\exp\left(-s\sum_{b'\in\Phi_b'}P_0H_{b',w}R_{b',w}^{-\alpha}\right)\right]\\&\overset{(a)}{=}\mathbb{E}_{R_{b',w}}\left[\mathbb{E}_{H_{b',w}}\left[\exp\left(-s\sum_{b'\in\Phi_b'}P_0H_{b',w}R_{b',w}^{-\alpha}\right)\right]\right]\\&\overset{(b)}{=}\mathbb{E}_{R_{b',w}}\left[\prod_{b'\in\Phi_b'}\mathbb{E}_{H_{b',w}}\left(\exp\left(-sP_0R_{b',w}^{-\alpha}H_{b',w}\right)\right)\right]\\&\overset{(c)}{=}\mathbb{E}_{R_{b',w}}\left[\prod_{b'\in\Phi_b'}\int_0^{\infty}\exp\left[-g(b',w)h_{b',w}\right]f\left(h_{b',w}\right)dh_{b',w}\right]\\&\overset{(d)}{=}\mathbb{E}_{R_{b',w}}\left[\prod_{b'\in\Phi_b'}\int_0^{\infty}\exp\left[-g(b',w)h_{b',w}\right]\mu\exp\left(-\mu h_{b',w}\right)dh_{b',w}\right]\\&=\mathbb{E}_{R_{b',w}}\left[\prod_{b'\in\Phi_b'}\left(\frac{\mu}{\mu+g(b',w)}\right)\right]\end{aligned}\tag{10}$$

In (10), Eq. (a) holds because $R_{b',w}$ and $H_{b',w}$ are mutually independent. Eq. (b) is due to the exponentiation identity. Eq. (c) follows from the definition of expectation of $R_{b',w}$, where $g(b',w)\triangleq sP_0R_{b',w}^{-\alpha}$, and $R_{b',w}=\|b'-w\|$. Eq. (d) holds because $H_{b',w}$ is exponentially distributed with mean $1/\mu$, i.e., $f\left(h_{b',w}\right)=\mu\exp\left(-\mu h_{b',w}\right)$. Recall that (i) the interfering tags Φ_b' of node w do not include the tags in the subcell of the transmitting node (i.e., subcell $\mathcal{S}_1$) and in the subcell of node w (i.e., subcell $\mathcal{S}_2$); (ii) the location of interfering tags Φ_b' also depends on the location of non-transmitting nodes in the set of $\Phi_{w'}$. However, like [4], [5], we may regard Φ_b' as an MCP with mean $\overline{\Psi}$ tags in each subcell, i.e., average $\overline{\Psi}$ concurrently transmitting tags in each subcell. Let $v(b')\triangleq\frac{\mu}{\mu+g(b',w)}$. With the help of Figs. 2 and 4 in the paper, according to the PGFL of MCP, the last equation of (10) becomes

$$\mathcal{L}_I(s)=\mathbb{E}\left[\prod_{b'\in\Phi_b'}v(b')\right]=\exp\left(-\lambda_w'\int_{\mathcal{A}}\left[1-\exp\left(-\overline{\Psi}\int_{\mathcal{B}}\left(1-v(b''+w')\right)f(b''|w')db''\right)\right]dw'\right)\tag{11}$$

where w' is the node with interfering tag b'' located within its subcell, λ_w' is the density of $\Phi_{w'}$, and $\mathcal{A}$ is the area in which the node w' locate. Recall that $\mathcal{A}$ excludes the subcell of the transmitting node (i.e., subcell $\mathcal{S}_1$) and the subcell of node w (i.e., subcell $\mathcal{S}_2$) in one cell. For the ease of analysis, we approximate $\mathcal{A}$ by a circular disk $\mathcal{D}(w,d)$ centered at node w with radius d. $\mathcal{B}$ is the area in which the interfering tags b'' locate. We express $\mathcal{B}$ as a circular disk $\mathcal{D}\left(w',\tilde{d}\right)$ centered at node w' with radius $\tilde{d}$. It should be noted that b'' is the Cartesian coordinate with respect to w', which is a different coordinate representation of b' under different reference points. Hence, we can use $b''+w'$ to express b'.

In (11), $v(b''+w')$ can be further expressed as

$$(b''+w')=\frac{\mu}{\mu+sP_0\|b''+w'-w\|^{-\alpha}}=\frac{\mu}{\mu+sP_0\|b'-w\|^{-\alpha}}.\tag{12}$$

Set $\mu=1$, i.e., $H\sim\mathrm{Exp}(1)$. Then we convert (11) from Cartesian coordinates to polar coordinates [5], [6], i.e.,

$$\mathcal{L}_I(s)=\exp\left(-2\pi\lambda_w'\int_{\check{d}}^{\tilde{d}}\left(1-\Delta_1\right)R_{w',w}dR_{w',w}\right)\tag{13}$$

in which

$$\begin{aligned}\Delta_1&=\exp\left(-\overline{\Psi}\int_0^{\infty}\frac{\|b'-w\|^{-\alpha}}{(sP_0)^{-1}+\|b'-w\|^{-\alpha}}\tilde{f}_{R_{b',w}}\left(r_{b',w}\middle|R_{w',w}\right)dr_{b',w}\right)\\&=\exp\left(-\overline{\Psi}\int_0^{\infty}\frac{r_{b',w}^{-\alpha}}{\left(\theta r_{b,w}^{\alpha}\right)^{-1}+r_{b',w}^{-\alpha}}\tilde{f}_{R_{b',w}}\left(r_{b',w}\middle|R_{w',w}\right)dr_{b',w}\right)\end{aligned}\tag{14}$$

where $\tilde{f}_{R_{b',w}}(r_{b',w}|R_{w',w})$ is the conditional probability density function of the distance between interfering tags b' and receiver node w. Then, we can express $\tilde{f}_{R_{b',w}}(r_{b',w}|R_{w',w})$ as

$$\tilde{f}_{R_{b',w}}(r_{b',w}|R_{w',w}) = \begin{cases} \frac{\Delta_2}{\pi \tilde{d}^2} & r_{b',w} \in [\check{r}, \hat{r}] \\ 0 & \text{otherwise} \end{cases} \tag{15}$$

where $\check{r} = r_{w',w} - \tilde{d}$, $\hat{r} = r_{w',w} + \tilde{d}$, Δ_2 is the arc as shown in Fig. 4 in the paper, and the distance between the interfering tags b' lying on Δ_2 and w is always same. In our work, we set $\check{d} \geq \tilde{d}$, i.e., $\check{r} \geq 0$ to avoid the distance between any two nodes too close. Then we can express Δ_2 as

$$\Delta_2 = 2r_{b',w} \arccos\left(\frac{r_{w',w}^2 + r_{b',w}^2 - \tilde{d}^2}{2r_{w',w}r_{b',w}}\right) \tag{16}$$

Numerical evaluation on the integral form of (13) is time consuming and may not provide significant insights. To address this, we present an asymptotic analysis for $\mathcal{L}_I(s)$ below.

Asymptotic lower bound: When $\check{d} \to 0, d \to \infty$, [7] gives a closed-form lower bound to approximate the value of Laplace transform of interference I. Adopting the method in [7], we can obtain a lower bound of (13) as follows:

$$\begin{aligned}
\mathcal{L}_I(s) &= \exp\left(-2\pi\lambda'_w \int_0^\infty (1-\Delta_1)\, R_{w',w} dR_{w',w}\right) \\
&\overset{(a)}{\geq} \exp\left(-2\pi\lambda'_w \int_0^\infty \int_0^\infty \frac{\bar{\Psi} r_{b',w}^{-\alpha}}{\left(\theta r_{b,w}^{\alpha}\right)^{-1} + r_{b',w}^{-\alpha}} \tilde{f}_{R_{b',w}}(r_{b',w}|R_{w',w}) dr_{b',w}\, R_{w',w} dR_{w',w}\right) \\
&\overset{(b)}{=} \exp\left(-2\pi\lambda'_w \bar{\Psi} \int_0^\infty \frac{r_{b',w}^{-\alpha}}{\left(\theta r_{b,w}^{\alpha}\right)^{-1} + r_{b',w}^{-\alpha}} r_{b',w} dr_{b',w}\right) \\
&\overset{(c)}{=} \exp\left(-2\pi\lambda'_w \bar{\Psi} r_{b,w}^2 \theta^{\frac{2}{\alpha}} \int_0^\infty \frac{y}{1+y^\alpha} dy\right) \\
&\overset{(d)}{=} \exp\left(-2\pi\lambda'_w \bar{\Psi} r_{b,w}^2 \theta^{\frac{2}{\alpha}} \cdot \frac{1}{\alpha} \cdot \Gamma\left(\frac{2}{\alpha}\right) \cdot \Gamma\left(1-\frac{2}{\alpha}\right)\right) \\
&\overset{(e)}{=} \exp\left(-\lambda_p \bar{c} r_{b,w}^2 \theta^{\frac{2}{\alpha}} \frac{2\pi^2}{\alpha \sin(2\pi/\alpha)}\right) \\
&\overset{(f)}{=} \exp\left(-\pi\lambda'_w \bar{\Psi} r_{b,w}^2 \theta^{\frac{2}{\alpha}} \frac{1}{\operatorname{sinc}(2/\alpha)}\right)
\end{aligned} \tag{17}$$

where Eq. (a) is from the fact that $1 - \exp(-ax) \leq ax$ for $a \geq 0$; Eq. (b) is because $\int_0^\infty \tilde{f}_{R_{b',w}}(r_{b',w}|R_{w',w}) R_{w',w} dR_{w',w} = \int_0^\infty \tilde{f}_{R_{b',w}}(R_{w',w}|r_{b',w}) r_{b',w} dR_{w',w} = r_{b',w}$ [7]; Eq. (c) follows by changing the variable $y^\alpha = \frac{1}{\theta r_{b,w}^{\alpha} r_{b',w}^{-\alpha}}$, i.e, $y = \frac{r_{b',w}}{r_{b,w}\theta^{\frac{1}{\alpha}}}$, and $y \in (0, \infty)$; Eq. (d) can refer to Eq. (3.241.4) in [8]. Eq. (e) follows from the Euler's reflection formula $\Gamma(x) \cdot \Gamma(1-x) = \frac{\pi}{\sin(\pi x)}$, where $\Gamma(x) = \int_0^\infty t^{x-1} e^{-t} dt\,, x > 0$ is the complete gamma function; Eq. (f) is from $\operatorname{sinc}(x) = \frac{\sin(\pi x)}{\pi x}$. In (17), the lower bound of $\mathcal{L}_I(s)$ depends on λ'_w and $\bar{\Psi}$. Below, we calculate them, respectively.

2) Calculation of λ'_w

Here, we calculate the density λ'_w of nodes w' forming the subcells that contain interfering tags of Φ'_b. Note that $\mathbb{E}(\Phi'_w(A))$ is the average number of interfering subcells in A when node w is receiving a desired tag transmission. We have

$$\lambda'_w = \frac{\mathbb{E}(\Phi'_w(A))}{|A|} \tag{18}$$

As shown in Fig. 2 in the paper, when N1 in $\mathcal{S}_1$ is transmitting a packet to the AP, tag b in $\mathcal{S}_2$ regards this transmitting signal as the excitation signal and contends for the channel. When tag b wins the channel and starts transmitting its data to node w, all other tags in $\mathcal{S}_2$ will not transmit. In addition, all tags in $\mathcal{S}_1$ will not transmit. Therefore, $\mathcal{S}_1$ and $\mathcal{S}_2$ are not interfering subcells. In one cell, all subcells except the two subcells are interfering subcells. Note that one node forms one subcell. We can express $\mathbb{E}(\Phi'_w(A))$ as

$$\mathbb{E}(\Phi'_w(A)) = \mathbb{E}(\Phi_w(A)) - 2 \tag{19}$$

where $\mathbb{E}(\Phi_w(A)) = \lambda_w |A|$ is the mean number of nodes in the cell.

3) Calculation of $\bar{\Psi}$

Let $\mathbb{E}(\Psi)$ be the mean of Ψ. Then we have

$$\bar{\Psi} \triangleq \mathbb{E}(\Psi) \tag{20}$$

Recall that the average number of interfering tags Ψ in each subcell is associated with the number of tags n in each subcell. Let $\mathbb{E}(\Psi|n)$ denote the average number of transmitting tags in one interfering subcell. Hence, we have

$$\mathbb{E}(\Psi) = \mathbb{E}\big(\mathbb{E}(\Psi|n)\big) = \sum_{n=1}^{\hat{n}} \mathbb{E}(\Psi|n) \cdot \mathbb{P}(n) \tag{21}$$

where $\mathbb{P}(n)$ is given in Eq. (23) in the paper and $\mathbb{E}(\Psi|n)$ is expressed as

$$\mathbb{E}(\Psi|n) = \sum_{\psi=1}^{n} \psi \cdot \mathbb{P}(\Psi = \psi|n) \tag{22}$$

where $\mathbb{P}(\Psi = \psi|n)$ is given in Eq. (24) in the paper.

Appendix F: Details of TABLE II

Here, we list the default parameter settings of simulation in Table II.

TABLE II
DEFAULT PARAMETER VALUES

Parameters	Description	Value
R_{data}	Data Rate of MCS 8	7.8 Mbps
R_{basic}	Basic Rate	0.65 Mbps
T_{SIFS}	Duration of one SIFS interval	160 μs
T_{DIFS}	Duration of one DIFS interval	264 μs
ω	Duration of a basic slot	52 μs
L_w	WiFi packet size	1000 *bytes*
PHY Header	Duration of PHY header	160 μs
MAC Header	(40bytes+4bytes) @R_{data}	46 μs
Route Header	20bytes@R_{data}	21 μs
Header	PHY + MAC + Route Header	227 μs
T_w	1000bytes@R_{data}	1026 μs
L_b	Backscatter packet size	26 bits
T_{ACK}	(24bytes+14bytes) @R_{basic}	39 μs
$T_{ACKTimeout}$	ACKTimeout time	199 μs
$\check{C}$	Minimum contention window size	16
K	Maximum backoff stage	7
L	Number of busy tones	8
T_{tone}	Duration of each busy tone	16 μs
d	Radius of one cell	100 m

Appendix G: Successful Transmission Probability $\mathbb{P}_b^s$ of a Tag

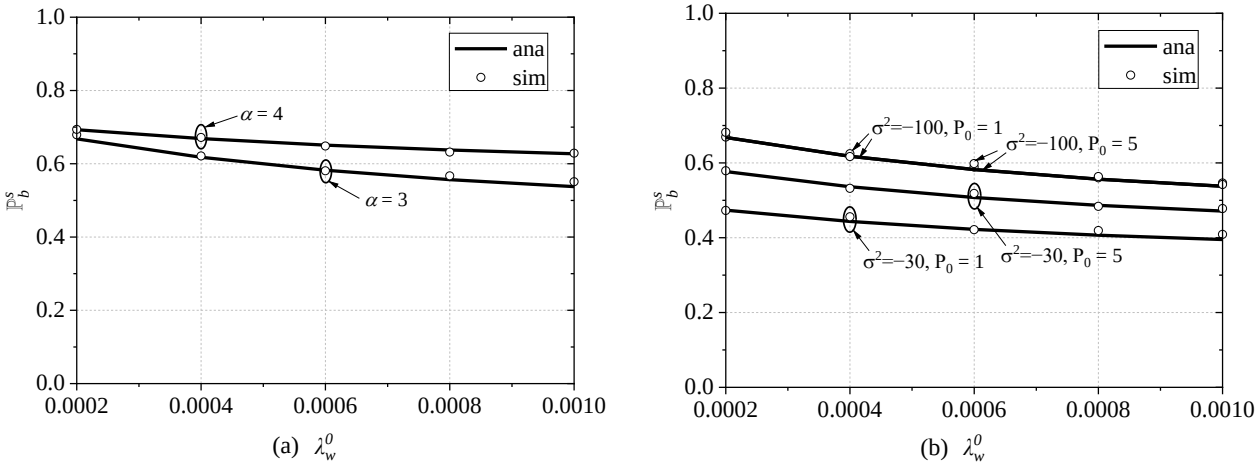

Fig. 3. $\mathbb{P}_b^s$ versus λ_w^0 with (a) $\alpha = 3, 4$, P_0 =1 dBm and $\sigma^2 = -100$ dBm; (b) $\alpha = 3$, $\sigma^2 = -100, -30$ dBm, and $P_0 = 1, 5$ dBm.

Figs. 3(a)-(b) show the impacts of different path-loss exponent α, reflection power P_0, and noise power σ^2 on $\mathbb{P}_b^s$ as λ_w^0 varies from 0.0002 to 0.001 nodes/m^2. Besides, $\check{d}$ = 10 m, $L = 8$, $\Lambda_b = 5$ and $\theta = 10$ dB. From these two subfigures, we can conclude:

- Given α, P_0, and σ^2, $\mathbb{P}_b^s$ decreases as λ_w^0 increases, as shown in Figs. 3(a)-(b). The reason is as follows. In this setting, as λ_w^0 increases, λ_w does, the number of interfering links increases and hence the successful transmission probability $\mathbb{P}_b^s$ decreases.
- Given λ_w^0, P_0, and σ^2, the larger α, the higher $\mathbb{P}_b^s$ as shown in Fig. 3(a). The reason is that when α is large, the power of interfering signals received at the receiver is small, which leads to a high SINR and a high $\mathbb{P}_b^s$.

- Given α, λ_w^0 and P_0, $\mathbb{P}_b^s$ increases as σ^2 decreases, while given α, λ_w^0 and σ^2, $\mathbb{P}_b^s$ increases as P_0 increases, as shown in Fig. 3(b). The reason is that decreasing σ^2 and increasing P_0 can increase SINR and hence $\mathbb{P}_b^s$.
- Given α and λ_w^0, when σ^2 decreases from -30 to -100 dBm, $\mathbb{P}_b^s$ increases significantly if P_0 is small (e.g., $P_0 = 1$ dBm) and increases slightly if P_0 is large (e.g., $P_0 = 5$ dBm), as shown in Fig. 3(b). This indicates that σ^2 has a strong impact on $\mathbb{P}_b^s$ if P_0 is small.
- Given α and λ_w^0, when we improve P_0 from 1 to 5 dBm, $\mathbb{P}_b^s$ remains almost unchanged if σ^2 is very small (e.g., $\sigma^2 = -100$ dBm) and increases rapidly if σ^2 is large (e.g., $\sigma^2 = -30$ dBm), as shown in Fig. 3(b). This implies that increasing P_0 is not an effective solution of improving $\mathbb{P}_b^s$ if σ^2 is small.

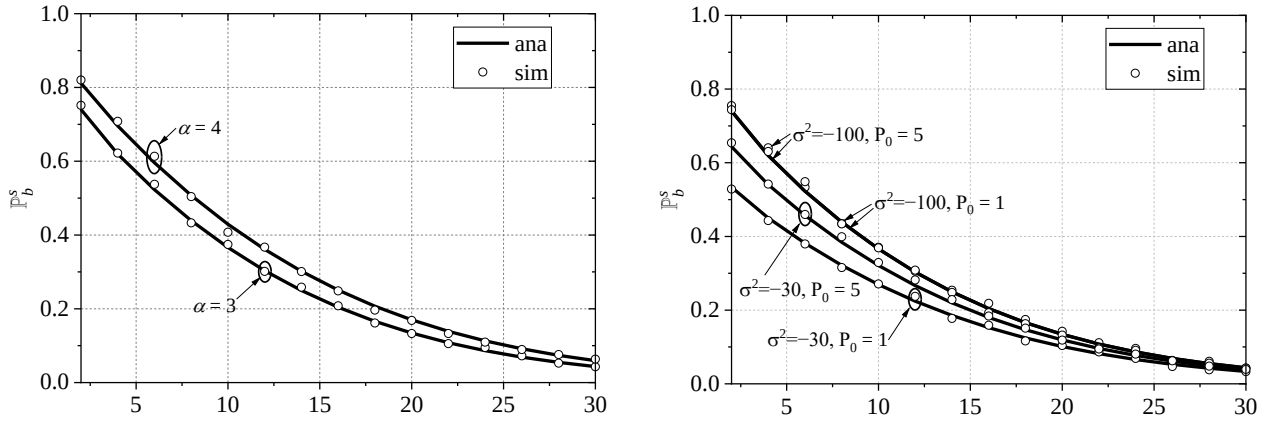

(a) Λ_b (b) Λ_b

Fig. 4. $\mathbb{P}_b^s$ versus Λ_b with (a) $\alpha = 3, 4$, $\check{d}$ = 10 m, $P_0 = 1$ dBm, and $\sigma^2 = -100$ dBm and (b) $\alpha = 3$, $\check{d}$ = 10 m, $P_0 = 1, 5$ dBm and $\sigma^2 = -100, -30$ dBm.

Figs. 4(a)-(b) plot the impacts of different α, P_0, and σ^2 on $\mathbb{P}_b^s$ as Λ_b varies from 2 to 30. Besides, $\lambda_w^0 = 0.0005$ nodes/m^2, $\check{d}$ = 10 m, $L = 8$, $\theta = 10$ dB. From these subfigures, we have similar observations as in Figs. 3(a)-(b), which are omitted.

Appendix G: Verification of $\mathbb{P}(\boldsymbol{\Psi} = \boldsymbol{\psi}|\boldsymbol{n})$ and $\bar{\boldsymbol{\Psi}}$

We respectively verify the accuracy of $\mathbb{P}(\Psi = \psi|n)$ of (24) in the paper and $\bar{\Psi}$ of (*20*) as the number of tags n and the mean number of tags Λ_b in a subcell varies under different setting of the number of busy tones L.

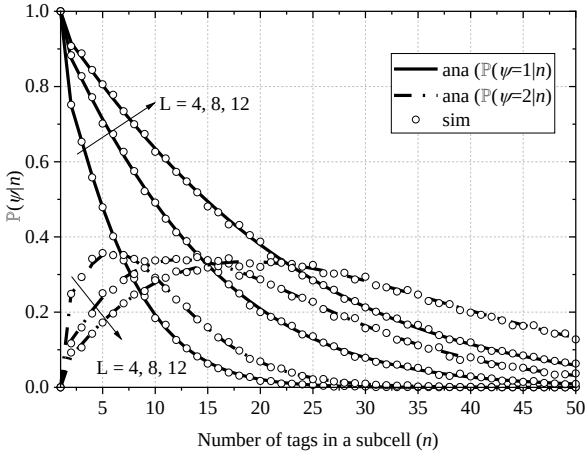

Fig. 5. $\mathbb{P}(\Psi = \psi|n)$ versus n under $L = 4, 8, 12$.

Fig. 5 shows the impacts of different L (i.e., $L = 4, 8, 12$) on $\mathbb{P}(\Psi = \psi|n)$ with $\psi = 1, 2$, as n varies from 1 to 50. From this figure, we can conclude:

- Given L, as n increases, $\mathbb{P}(\Psi = 1|n)$ decreases. It is because that more tags in a subcell lead to more serious contention. The probability of only one tag winning the contention gradually decreases. While as n increases, $\mathbb{P}(\Psi = 2|n)$ first increases for more contention, and then gradually decreases for more tags (i.e., $\Psi > 2$) concurrently wining the contention. Besides, the tendency of the curve of the probability $\mathbb{P}(\Psi = \psi|n)$ with $\Psi > 2$ is the same as that of $\mathbb{P}(\Psi = 2|n)$ and omitted.
- Given n, the larger L, the larger $\mathbb{P}(\Psi = 1|n)$. It is because for larger L, the tags have more possibilities to choose different backoff counters, and fewer tags choose the same minimum one. Thus, the probability of only one tag winning the contention is higher.

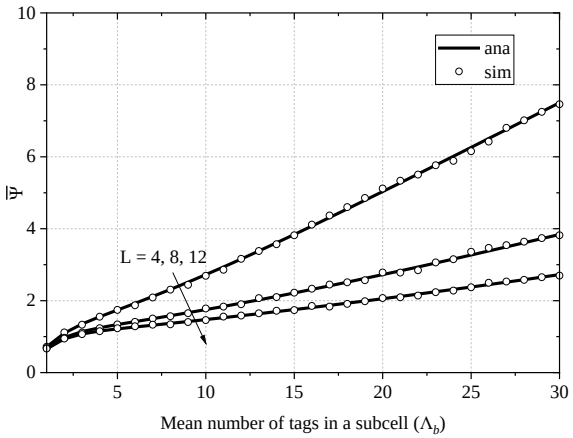

Fig. 6. $\bar{\Psi}$ versus Λ_b under $L = 4, 8, 12$.

Fig. 6 shows the impacts of different L (i.e., $L = 4, 8, 12$) on $\bar{\Psi}$ as Λ_b varies from 1 to 30. From this figure, we can conclude:

- Given L, $\bar{\Psi}$ increases as Λ_b increases. It is because a larger Λ_b means more tags in a subcell, and thus more tags may concurrently win the contention and transmit data.
- Given Λ_b, the larger L, the smaller $\bar{\Psi}$. The reason is the same as that in Fig. 5 and omitted.

Reference

[1] G. Bianchi, "Performance analysis of the IEEE 802. 11 distributed coordination function," *IEEE Journal on selected areas in communications*, vol. 18, no. 3, pp. 535–547, 2000.

[2] A. Kumar, E. Altman, D. Miorandi, and M. Goyal, "New Insights From a Fixed-Point Analysis of Single Cell IEEE 802.11 WLANs," *IEEE/ACM Transactions on Networking*, vol. 15, no. 3, pp. 588–601, Jun. 2007, doi: 10.1109/TNET.2007.893091.

[3] Z. Ma, L. Feng, and F. Xu, "Design and analysis of a distributed and demand-based backscatter MAC protocol for internet of things networks," *IEEE Internet of Things Journal*, vol. 6, no. 1, pp. 1246–1256, 2018.

[4] K. Han and K. Huang, "Wirelessly Powered Backscatter Communication Networks: Modeling, Coverage, and Capacity," *IEEE Transactions on Wireless Communications*, vol. 16, no. 4, pp. 2548–2561, Apr. 2017, doi: 10.1109/TWC.2017.2665629.

[5] J. Tang, G. Chen, J. P. Coon, and D. E. Simmons, "Distance distributions for Matérn cluster processes with application to network performance analysis," in *2017 IEEE International Conference on Communications (ICC)*, May 2017, pp. 1–6. doi: 10.1109/ICC.2017.7997055.

[6] Q. Wang, Y. Zhou, H.-N. Dai, G. Zhang, and W. Zhang, "Performance on Cluster Backscatter Communication Networks with Coupled Interferences," *IEEE Internet of Things Journal*, vol. 9, no. 20, pp. 20282–20294, Oct. 2022, doi: 10.1109/JIOT.2022.3174002.

[7] J. Tang, G. Chen, and J. P. Coon, "Joint Coverage Enhancement by Power Allocation in Poisson Clustered Out-of-Band D2D Networks," *IEEE Transactions on Vehicular Technology*, vol. 67, no. 12, pp. 11537–11548, Dec. 2018, doi: 10.1109/TVT.2018.2871065.

[8] I. S. Gradshteĭn, I. M. Ryzhik, and A. Jeffrey, *Table of integrals, series, and products*, 7th ed. Amsterdam ; Boston: Academic Press, 2007.

[9] Y. Wang, Q. Zhao, S. Yao, L. Feng, and H. Liang, "Performance Modeling of Tags-to-WiFi Transmissions for Contention-based WiFi Backscatter Networks," in *2022 IEEE International Conference on Networking, Sensing and Control (ICNSC)*, Dec. 2022, pp. 1–6. doi: 10.1109/ICNSC55942.2022.10004070.